


## Article

# Catalytic Wet Peroxide Oxidation of Anionic Pollutants over Fluorinated Fe<sub>3</sub>O<sub>4</sub> Microspheres at Circumneutral pH Values

Fengxi Chen <sup>1,\*</sup> , Huaixiang Lv <sup>1</sup>, Wu Chen <sup>2</sup> and Rong Chen <sup>1,3</sup>

<sup>1</sup> State Key Laboratory of New Textile Materials & Advanced Processing Technologies, Wuhan Textile University, Wuhan 430200, China

<sup>2</sup> School of Chemistry and Environmental Engineering, Wuhan Institute of Technology, Wuhan 430205, China

<sup>3</sup> Henan Institute of Advanced Technology, Zhengzhou University, Zhengzhou 450002, China

\* Correspondence: fxchen@wtu.edu.cn

**Abstract:** Fluorinated Fe<sub>3</sub>O<sub>4</sub> microspheres with 7.1 ± 1.4 wt% of fluoride (F-Fe<sub>3</sub>O<sub>4</sub>-1) were prepared via glycothermal synthesis. Fluorination significantly enhanced the activity of F-Fe<sub>3</sub>O<sub>4</sub>-1 in catalytic wet peroxide oxidation of anionic dyes (including orange G (OG) and congo red) at pH ~7. However, the promotional effect of fluorination became less obvious for amphoteric rhodamine B and was not observed for cationic methylene blue. After reacting with H<sub>2</sub>O<sub>2</sub> (40 mM) for 2 h at pH 6.5 and 40 °C, the decolorization rates of OG (0.1 mM) and the pseudo-first-order rate constant were 96.8% and 0.0284 min<sup>-1</sup> over F-Fe<sub>3</sub>O<sub>4</sub>-1 versus 17.6% and 0.0011 min<sup>-1</sup> over unmodified Fe<sub>3</sub>O<sub>4</sub>. The effects of reaction parameters (initial H<sub>2</sub>O<sub>2</sub> concentration and pH value and reaction temperature) on OG decolorization with H<sub>2</sub>O<sub>2</sub> over F-Fe<sub>3</sub>O<sub>4</sub>-1 were investigated. The reusability of F-Fe<sub>3</sub>O<sub>4</sub>-1 was demonstrated by OG decolorization in eight consecutive runs. Fluorination increased the isoelectric point of F-Fe<sub>3</sub>O<sub>4</sub>-1 to 8.7 and facilitated the adsorption and degradation of anionic dyes on the surface of F-Fe<sub>3</sub>O<sub>4</sub>-1 at pH ~7. Scavenging tests and EPR spectra supported that hydroxyl radicals were the main reactive species for the OG decolorization over F-Fe<sub>3</sub>O<sub>4</sub>-1.

**Keywords:** magnetite; fluorination; wastewater treatment; Fenton-like oxidation; anionic dyes; adsorption



**Citation:** Chen, F.; Lv, H.; Chen, W.; Chen, R. Catalytic Wet Peroxide Oxidation of Anionic Pollutants over Fluorinated Fe<sub>3</sub>O<sub>4</sub> Microspheres at Circumneutral pH Values. *Catalysts* **2022**, *12*, 1564. <https://doi.org/10.3390/catal12121564>

Academic Editors: Enric Brillas and Helder T. Gomes

Received: 7 November 2022

Accepted: 30 November 2022

Published: 2 December 2022

**Publisher's Note:** MDPI stays neutral with regard to jurisdictional claims in published maps and institutional affiliations.



**Copyright:** © 2022 by the authors. Licensee MDPI, Basel, Switzerland. This article is an open access article distributed under the terms and conditions of the Creative Commons Attribution (CC BY) license (<https://creativecommons.org/licenses/by/4.0/>).

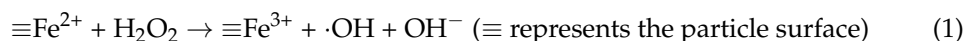
## 1. Introduction

Organic compounds constitute one of the most common pollutants found in wastewater that pose potential hazards to the ecosystem and the environment. Fenton oxidation is effective for organic wastewater remediation since it can generate strongly oxidative hydroxyl radicals ( $\bullet\text{OH}$ ,  $E^0 = 2.80\text{ V}$ ) that are capable of degrading most recalcitrant organic pollutants. However, the Fenton process requires acidic condition (pH ~3) and generates undesired iron sludge. Catalytic wet peroxide oxidation (CWPO) may overcome these problems since it can work at circumneutral pH values and avoid the formation of iron sludge [1–4]. However, most heterogeneous Fenton-like catalysts exhibit lower activity than the conventional homogeneous Fenton process [2,5–8] since the kinetics of a heterogeneous catalytic reaction are also affected by the mass transfer process inside the reaction system (e.g., adsorption and diffusion) besides the intrinsic activity of a catalyst. In this regard, the development of highly active and stable heterogeneous Fenton-like catalysts with favorable mass transfer is critical for a successful CWPO process.

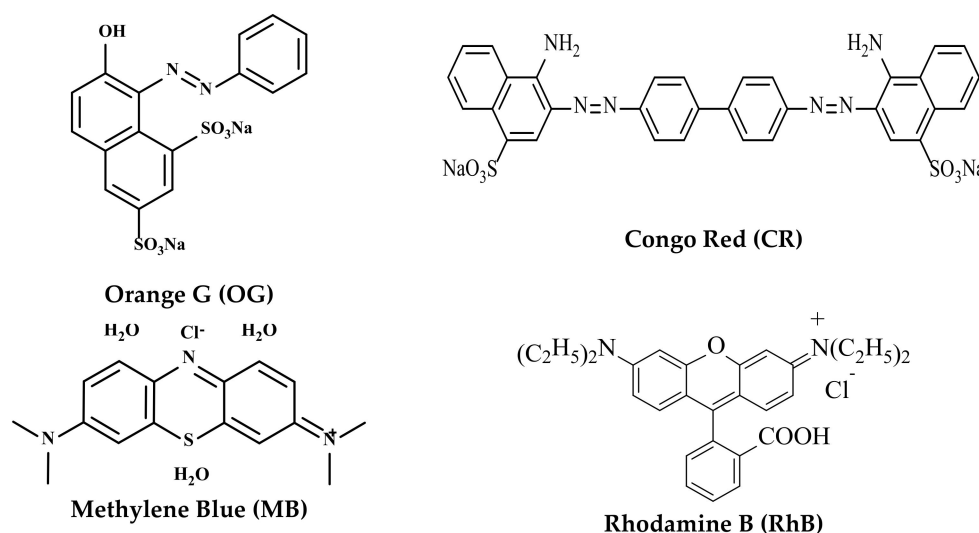
Magnetite (Fe<sub>3</sub>O<sub>4</sub>) is a promising heterogeneous Fenton-like catalyst owing to its intrinsic peroxidase-like activity and efficient magnetic separation [2,9–12]. However, it exhibits very low catalytic activity for the degradation of anionic organic contaminants under circumneutral pH conditions [10,13]. One reason for this is its low isoelectric point (IEP, about 6–7) [14–16]. As such, Fe<sub>3</sub>O<sub>4</sub> particles are negatively charged at pH ~7 and cannot effectively adsorb anionic contaminants due to electrostatic repulsion [14]. In addition, the activity of Fe<sub>3</sub>O<sub>4</sub> particles in activating H<sub>2</sub>O<sub>2</sub> under mild conditions (e.g., pH

~7 and room temperature) is still too weak and has to be further improved for practical applications [2].

Doping is a simple and useful methodology to enhance the activity of magnetite, wherein metallic dopants (e.g.,  $\text{Ti}^{4+}$ ,  $\text{Cu}^{2+}$ , and  $\text{Cr}^{3+}$ ) are the most commonly used [2,6,14,17,18]. In sharp contrast, nonmetal-doped  $\text{Fe}_3\text{O}_4$  have been seldom investigated. Fluoride doping is known for modulating semiconductor band structures with improved photocatalytic performances (e.g., F-doped  $\text{TiO}_2$ ,  $\text{SnO}_2$ ,  $\text{Co}_3\text{O}_4$ ,  $\gamma\text{-Fe}_2\text{O}_3$ ,  $\text{Cu}_2\text{O}$ , and  $\text{Bi}_2\text{WO}_6$  [19–24]). In fluorinated  $\text{Fe}_3\text{O}_4$  (F- $\text{Fe}_3\text{O}_4$ ) microspheres [25], fluoride may replace lattice oxygen or coordinate with surface lattice iron via ligand exchange with hydroxide groups. The substitution of lattice  $\text{O}^{2-}$  with  $\text{F}^-$  results in a framework with extra positive charge due to a charge imbalance. A number of possibilities exist for charge compensation, including by attracting anions (e.g.,  $\text{OH}^-$ ,  $\text{F}^-$ , and  $\text{Cl}^-$ ) from the solution, by reducing the average valence of the iron cations (e.g., increasing the content of low-valence ferrous ( $\text{Fe}^{2+}$ ) ions), or by introducing some cationic vacancies. Therefore, fluorination presents largely unexplored opportunities for adjusting the physicochemical properties of F- $\text{Fe}_3\text{O}_4$  for specific applications, e.g., it is expected to increase the surface zeta potential of the pristine  $\text{Fe}_3\text{O}_4$  for the enhanced adsorption of anionic compounds via electrostatic attraction and to improve the  $\text{H}_2\text{O}_2$ -activation capability via the Fenton-like reaction (Equation (1)).



In this work, we found that in comparison with unmodified  $\text{Fe}_3\text{O}_4$ , fluorination significantly enhanced the catalytic activity of F- $\text{Fe}_3\text{O}_4$  microspheres for the degradation of anionic pollutants (e.g., orange G (OG) and congo red (CR) in Scheme 1). However, this promotional effect became less obvious for an amphoteric dye rhodamine B (RhB), and no promotion was observed for a cationic dye methylene blue (MB)). The different activities of F- $\text{Fe}_3\text{O}_4$  in the degradation of cationic and anionic dyes were mainly attributed to the adsorption-enhanced catalytic oxidation of anionic dyes on its surface via a free-radical reaction pathway.



**Scheme 1.** Molecular structures of representative organic dyes used in this work.

## 2. Results and Discussion

### 2.1. Catalytic Performances of F- $\text{Fe}_3\text{O}_4$ -r Microspheres

As shown in Figure 1a, fluorination significantly enhanced the decolorization rate (DR) of OG (0.1 mM) with  $\text{H}_2\text{O}_2$  (40 mM) after reacting for 2 h at pH 6.5 and 40 °C over F- $\text{Fe}_3\text{O}_4$ -r (e.g., the 2 h DR increased from 17.6% for  $\text{Fe}_3\text{O}_4$ -blank to 62.2% for F- $\text{Fe}_3\text{O}_4$ -0.1). The best performance (96.8% of DR after 2 h) was obtained over F- $\text{Fe}_3\text{O}_4$ -1. A further

increase in the fluoride content resulted in a gradual decrease in the 2 h DRs of OG (0.1 mM) (68.4% for F-Fe<sub>3</sub>O<sub>4</sub>-2 and 47.5% for F-Fe<sub>3</sub>O<sub>4</sub>-3), which may be related to the increase in the Na<sub>3</sub>FeF<sub>6</sub> impurity in F-Fe<sub>3</sub>O<sub>4</sub>-r (r = 2, 3) [25]. By assuming that the instantaneous concentration of  $\bullet\text{OH}$  is constant since the amount of H<sub>2</sub>O<sub>2</sub> is in larger excess with regard to OG (40 mM vs. 0.1 mM), the decolorization process of OG in water was well fitted with the pseudo-first-order kinetic model ( $R^2$ : 0.990–0.997 in Figure 1b). The rate constants,  $k_{s1}$ , were obtained from the slopes of the straight lines by linear regression of  $\ln(C_0/C_t)$ -time plots. The change of  $k_{s1}$  with fluorination is similar to that of the DR (Table 1). A 2.5-fold increment in  $k_{s1}$  was achieved from Fe<sub>3</sub>O<sub>4</sub>-blank to F-Fe<sub>3</sub>O<sub>4</sub>-1 (0.0011 vs. 0.0284 min<sup>−1</sup>) at 40 °C.

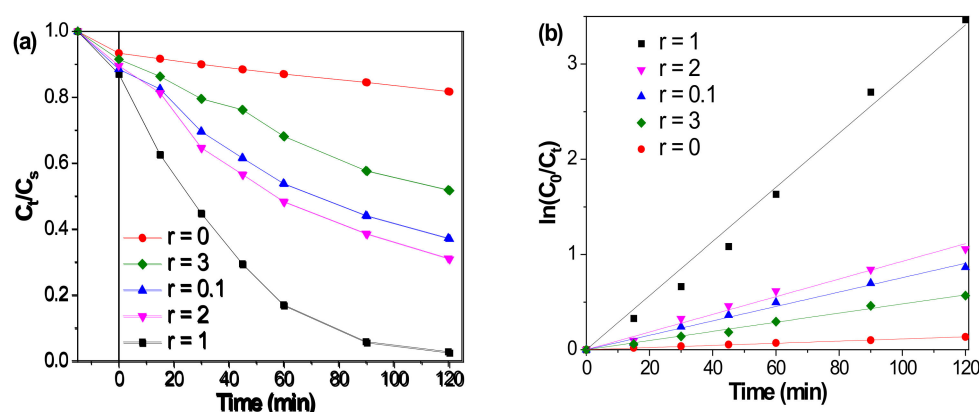


**Figure 1.** Catalytic degradation of OG with H<sub>2</sub>O<sub>2</sub> over F-Fe<sub>3</sub>O<sub>4</sub>-r (r = 0–3). (a)  $C_t/C_s$ -time plots and (b)  $\ln(C_0/C_t)$ -time plots. Reaction conditions: OG (0.1 mM, pH 6.8), H<sub>2</sub>O<sub>2</sub>: 40 mM, and catalyst loading: 0.5 g/L at 40 °C.

**Table 1.** Effect of fluorination on catalytic performances of F-Fe<sub>3</sub>O<sub>4</sub>-r microspheres for the OG decolorization <sup>1</sup>.

Entry	r	15-min Adsorption (%)	2-h DR (%)	$k_{s1}/\text{min}^{-1}$ ( $R^2$ )
1	0	5.9	17.6	0.0011 (0.997)
2	0.1	10.8	62.2	0.0070 (0.990)
3	1	12.3	96.8	0.0284 (0.991)
4	2	9.8	68.4	0.0092 (0.994)
5	3	7.8	47.5	0.0045 (0.991)
6 <sup>2</sup>	1	8.3	35.2	0.0026 (0.996)

<sup>1</sup> Reaction reactions were the same as Figure 1; <sup>2</sup> Tert-butanol (10 mM) added.

Shown in Figure 2a,b is the effect of the initial H<sub>2</sub>O<sub>2</sub> concentration,  $[\text{H}_2\text{O}_2]_0$ , on the decolorization of OG at 40 °C. The decolorization efficiency is lower at lower  $[\text{H}_2\text{O}_2]_0$ —the 2 h DR and  $k_{s1}$  value were only 65.9% and 0.0082 min<sup>−1</sup>, respectively, at 20 mM of  $[\text{H}_2\text{O}_2]_0$  in Table S1. On the other hand, higher  $[\text{H}_2\text{O}_2]_0$  was not beneficial either—the 2 h DE and  $k_{s1}$  value were 90.3% and 0.0182 min<sup>−1</sup>, respectively, at 80 mM of  $[\text{H}_2\text{O}_2]_0$ . The optimal  $[\text{H}_2\text{O}_2]_0$  was about 40–60 mM for efficient decolorization of OG (0.1 mM, pH 6.5) on F-Fe<sub>3</sub>O<sub>4</sub>-1 at 40 °C (the 2 h DE and  $k_{s1}$  value were ~97% and 0.030 min<sup>−1</sup>, respectively). The existence of the optimal H<sub>2</sub>O<sub>2</sub> concentration is due to the dual roles of H<sub>2</sub>O<sub>2</sub>. Firstly, it is the source of  $\bullet\text{OH}$  radicals for the OG degradation. Secondly, excess H<sub>2</sub>O<sub>2</sub> scavenges  $\bullet\text{OH}$  radicals (Equation (2)) [26,27], thus lowering the concentration of  $\bullet\text{OH}$  radicals in the solution.



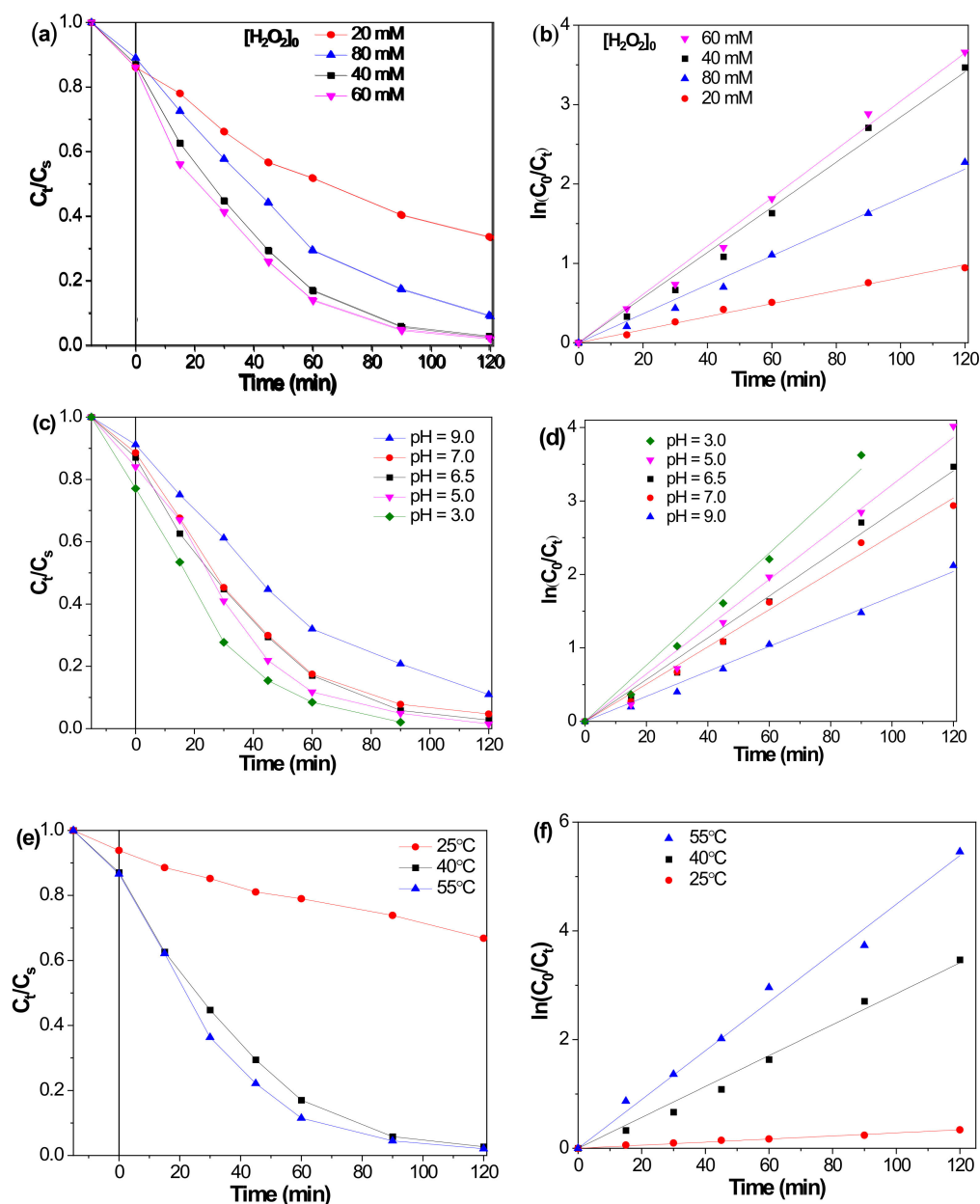


**Figure 2.** Effects of reaction parameters on OG decolorization with  $\text{H}_2\text{O}_2$  over  $\text{F-Fe}_3\text{O}_4\text{-1}$ . (a,c,e)  $C_t/C_s$ -time plots and (b,d,f)  $\ln(C_0/C_t)$ -time plots. General reaction conditions: OG (0.10 mM, pH 6.5),  $\text{H}_2\text{O}_2$ : 40 mM, and  $\text{F-Fe}_3\text{O}_4\text{-1}$ : 0.5 g/L at 40 °C for 2 h unless otherwise specified in the legends.

The OG decolorization at different pH values is presented in Figure 2c,d. Both the 2 h DR and  $k_{s1}$  value increased when the initial pH value reduced from 9.0 to 3.0. It is noteworthy that the high decolorization efficiencies of the OG (0.1 mM) solution could be achieved (2 h DR: 94.8–96.8% and  $k_{s1}$ : 0.0252–0.0284  $\text{min}^{-1}$  in Table S2) at the natural pH value of the OG (0.1 mM) solution (6.4–6.8). This has technological and operational advantages since it is not required to pre-adjust its pH value.

The temperature effect on the OG decolorization is displayed in Figure 2e,f. It is obvious that the 2 h DE and  $k_1$  value increased as the reaction temperature increased from 25 °C to 50 °C (e.g., they were 32.6% and 0.0028  $\text{min}^{-1}$  at 25 °C, and increased to 99.5% and 0.0445  $\text{min}^{-1}$  at 55 °C in Table S3). The kinetic parameters, including the activation energy ( $E_a$ ) and collision frequency ( $A$ , also called pre-exponential factor), of the OG decolorization, were estimated from the linear Arrhenius equation of  $\ln k_{s1} =$

$\ln A - E_a/RT$ , where  $R$  is the universal gas constant ( $8.314 \text{ J}/(\text{mol}\cdot\text{K})$ ). The  $E_a$  value was estimated to be  $75.7 \text{ kJ/mol}$  from the slope of the fitted linear equation of the plot of  $\ln k_{s1} - 1000/T$  (Figure S1), which is significantly lower than the dissociation energy of  $\text{H}_2\text{O}_2$  to  $\cdot\text{OH}$  ( $213.8 \text{ kJ/mol}$ ) due to the catalytic effect of  $\text{F-Fe}_3\text{O}_4\text{-1}$  [28] but higher than those obtained for the RhB degradation on  $\text{Fe}_3\text{O}_4$  MNPs ( $45.6 \text{ kJ/mol}$  [26],  $46.6 \text{ kJ/mol}$  [29],  $47.6 \text{ kJ/mol}$  [10] or  $51 \text{ kJ/mol}$  [30]), which may be attributed to the smaller surface area of the  $\text{F-Fe}_3\text{O}_4\text{-1}$  microspheres. However, it is interesting to note that the pre-exponential factor  $A$  in the reaction system of  $\text{OG}/\text{F-Fe}_3\text{O}_4\text{-1}$  microspheres is five orders of magnitude larger than that obtained in  $\text{RhB}/\text{Fe}_3\text{O}_4$  MNPs ( $6.88 \times 10^{10} \text{ min}^{-1}$  vs.  $8.26 \times 10^5 \text{ min}^{-1}$  [10]), which indicates that collision frequency between reacting species are greatly enhanced on  $\text{F-Fe}_3\text{O}_4\text{-1}$  microspheres in agreement with the proposed adsorption-enhanced catalytic degradation of anionic molecules (*vide infra*).

To check the scope of the applicability of  $\text{F-Fe}_3\text{O}_4\text{-1}$  in organic wastewater treatment, the CWPO degradations of other organic dyes (CR, MB, and RhB) were investigated and displayed in Figure 3 and Table 2. As shown in Figure 3a,b, the degradation of another anion dye CR was also significantly promoted on  $\text{F-Fe}_3\text{O}_4\text{-1}$  than on  $\text{Fe}_3\text{O}_4\text{-blank}$  (the 2 h DR and  $k_{s1}$  increased from 19.2% and  $0.0012 \text{ min}^{-1}$  for  $\text{Fe}_3\text{O}_4\text{-blank}$  to 91.7% and  $0.024 \text{ min}^{-1}$  for  $\text{F-Fe}_3\text{O}_4\text{-1}$ ). However, the promotional effect of fluorination was not observed for cationic dye MB (2 h DR and  $k_{s1}$ : 44.2% and  $0.0036 \text{ min}^{-1}$  on  $\text{Fe}_3\text{O}_4\text{-blank}$  versus 42.4% and  $0.0040 \text{ min}^{-1}$  on  $\text{F-Fe}_3\text{O}_4\text{-1}$ ) and became less obvious for the RhB dye (2 h DR and  $k_{s1}$ : 16.4% and  $0.0039 \text{ min}^{-1}$  on  $\text{Fe}_3\text{O}_4\text{-blank}$  versus 67.5% and  $0.0080 \text{ min}^{-1}$  on  $\text{F-Fe}_3\text{O}_4\text{-1}$ ). The  $pK_a$  value of RhB was reported to be 3.5 [31],  $4.1 \pm 0.1$  [32,33], or 6.41 [27]. Therefore, the carboxylic acid group of RhB is deprotonated and becomes negatively charged at the tested pH ( $\sim 6.6$ ), which may partially contribute to the enhanced adsorption and degradation of RhB on  $\text{F-Fe}_3\text{O}_4\text{-1}$ .

**Table 2.** CWPO of organic dyes over  $\text{F-Fe}_3\text{O}_4\text{-r}$  microspheres.

Organic Dyes	r	15-min Adsorption (%)	Degradation Rate (%)	$k_{s1}/\text{min}^{-1}$ ( $R^2$ )
CR (100 mg/L, pH 6.8)	0	5.2	19.2	0.0012 (0.975)
	1	34.3	91.7	0.024 (0.976)
MB (0.01 mM, pH 6.5)	0	11.6	44.2	0.0036 (0.989)
	1	7.3	42.4	0.0040 (0.990)
RhB (0.01 mM, pH 6.6)	0	17.4	49.3	0.0039 (0.984)
	1	16.6	67.1	0.0080 (0.993)

$\text{F-Fe}_3\text{O}_4\text{-1}$  maintained its high catalytic activity after continuously running for 16 h in recyclability tests (Figure 4 and Table 3). The 2 h DR,  $k_{s1}$ , and chemical oxygen demand (COD) reduction rate were 84.9%,  $0.0151 \text{ min}^{-1}$ , and 65.2%, respectively, in the eighth run of  $\text{F-Fe}_3\text{O}_4\text{-1}$ . The low-to-moderate COD reduction rate (65.2–83.2%) indicated the formation of some organic intermediates during the degradation of OG with  $\text{H}_2\text{O}_2$ . These intermediates may cover some active sites on  $\text{F-Fe}_3\text{O}_4\text{-1}$ , resulting in a gradual reduction in the activity of reused  $\text{F-Fe}_3\text{O}_4\text{-1}$ .

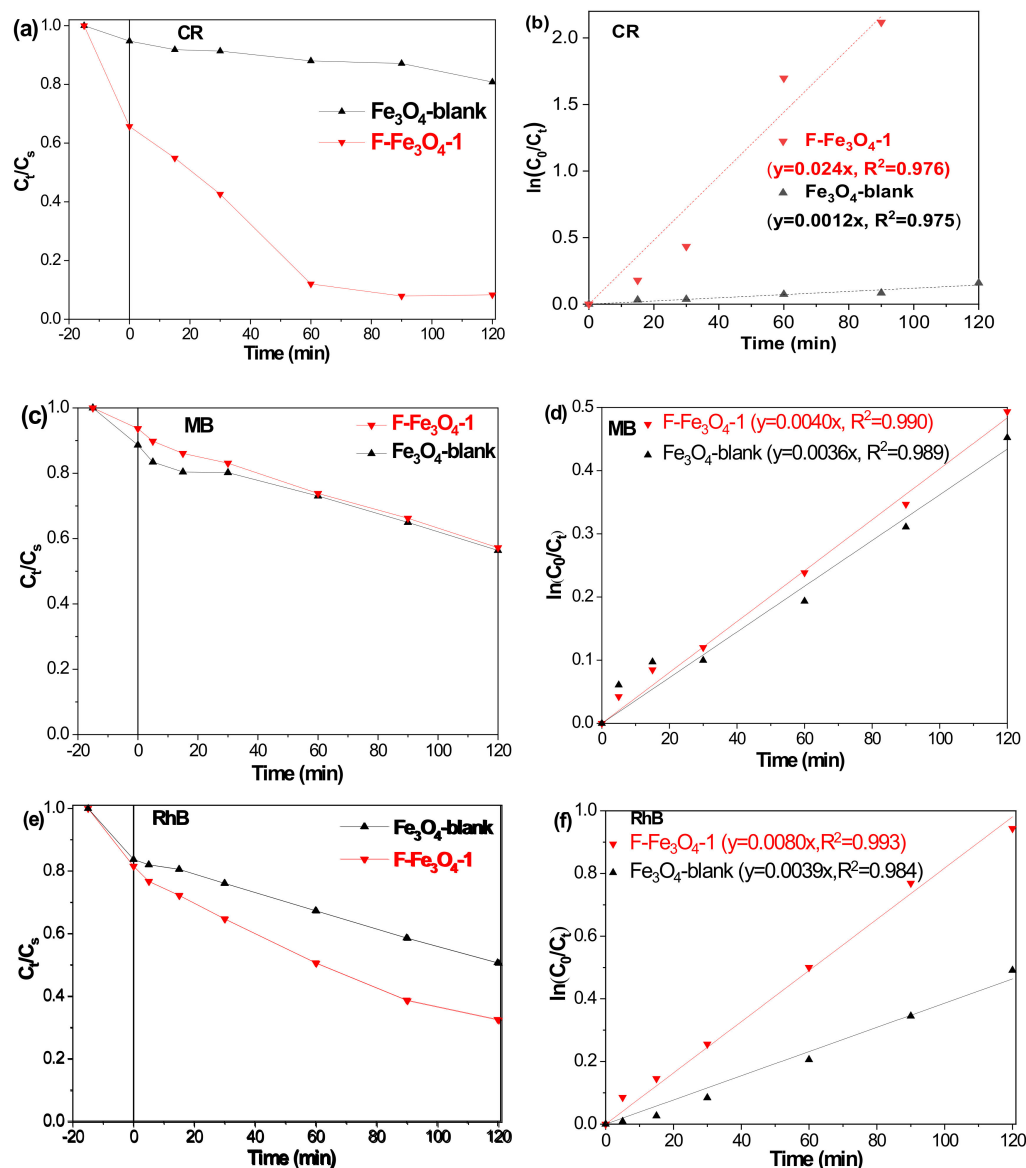


**Figure 3.** CWPO of organic dyes over F-Fe<sub>3</sub>O<sub>4</sub>-r (r = 0 and 1) microspheres. (a,c,e)  $C_t/C_s$ -time plots and (b,d,f)  $\ln(C_0/C_t)$ -time plots. Reaction conditions: CR (100 mg/L, pH 6.8) (MB (0.01 mM, 6.5) or RhB (0.01 mM, 6.6)), H<sub>2</sub>O<sub>2</sub>: 40 mM, catalyst loading: 0.5 g/L at 25 °C except 40 °C for CR.

**Table 3.** Recyclability of F-Fe<sub>3</sub>O<sub>4</sub>-1 for catalytic degradation of OG with H<sub>2</sub>O<sub>2</sub><sup>1</sup>.

Run	2-h DR (%)	$k_{s1}/\text{min}^{-1}$ ( $R^2$ )	COD Reduction Rate (%)
1	96.8	0.0284 (0.988)	83.2
2	92.7	0.0191 (0.978)	80.1
3	89.6	0.0178 (0.990)	75.5
4	89.1	0.0170 (0.988)	70.4
5	87.1	0.0163 (0.985)	68.6
6	86.4	0.0160 (0.990)	66.4
7	85.9	0.0157 (0.987)	66.1
8	84.9	0.0151 (0.987)	65.2

<sup>1</sup> Reaction conditions were the same as Figure 4.



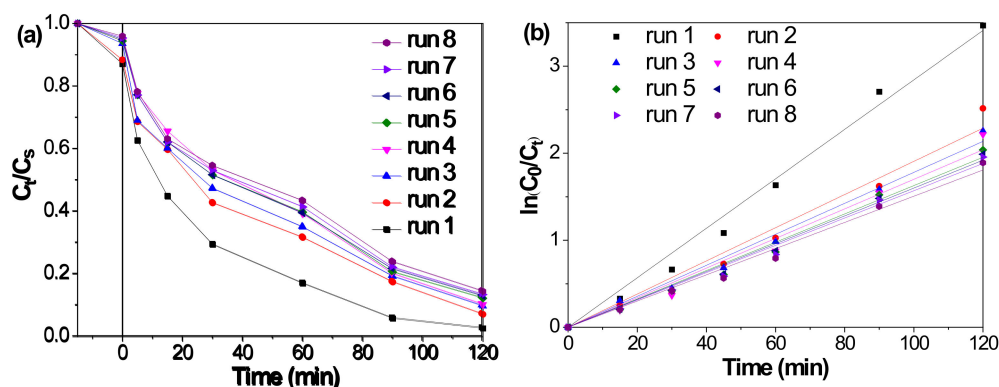


**Figure 4.** Recyclability tests of F-Fe<sub>3</sub>O<sub>4</sub>-1 for catalytic degradation of OG with H<sub>2</sub>O<sub>2</sub>. (a)  $C_t/C_s$ -time plots and (b)  $\ln(C_0/C_t)$ -time plots. Reaction conditions: fresh F-Fe<sub>3</sub>O<sub>4</sub>-1: 0.5 g/L, OG (0.1 mM, pH 6.5), and H<sub>2</sub>O<sub>2</sub>: 40 mM at 40 °C for 2 h. The used F-Fe<sub>3</sub>O<sub>4</sub>-1 was magnetically recovered and directly re-used as the fresh.

## 2.2. Characterization of F-Fe<sub>3</sub>O<sub>4</sub>-r Microspheres

The F-Fe<sub>3</sub>O<sub>4</sub>-r microspheres used in this work have been characterized in our previous work [25]. The XRD patterns shown in Figure 1 of Reference 25 indicate that F-Fe<sub>3</sub>O<sub>4</sub>-r ( $r \leq 1$ ) consist of the single magnetite (PDF #19-0629) phase while F-Fe<sub>3</sub>O<sub>4</sub>-r ( $r = 2, 3$ ) contain the Na<sub>3</sub>FeF<sub>6</sub> (PDF #22-1381) impurity. Unless otherwise specified, the fluorinated Fe<sub>3</sub>O<sub>4</sub> in this work referred to F-Fe<sub>3</sub>O<sub>4</sub>-1 microspheres, which comprise pure magnetite with the highest fluoride content ( $7.1 \pm 1.4$  wt% determined by EDX in Table S4) and the best catalytic performance (Figure 1). In comparison with Fe<sub>3</sub>O<sub>4</sub>-blank, F-Fe<sub>3</sub>O<sub>4</sub>-1 microspheres have a reduced average particle size ( $360 \pm 80$  nm vs.  $220 \pm 34$  nm) with slightly more aggregation (Figure 2 in Reference [25]), which resulted in their smaller  $S_{BET}$  value (28.0 and 17.6 m<sup>2</sup>/g) (Figure 3 in Reference [25]). However, there is no obvious change in the magnetic properties of Fe<sub>3</sub>O<sub>4</sub> upon fluorination (Figure 4 in Reference [25]), which is beneficial for the magnetic separation and recycling of the F-Fe<sub>3</sub>O<sub>4</sub>-1 microspheres.

## 2.3. Mechanistic Investigation

The concentrations of dissolved F<sup>−</sup> and iron ions after OG decolorization were, respectively, 0.65 mg/L and 0.15 mg/L, which meet the criteria set in the fourth edition of the World Health Organization's Guidelines for drinking-water quality (0.5–1 mg/L fluoride and <0.3 mg/L iron). In addition, the decolorization of OG (0.1 mM) was negligible (~5%) after replacing F-Fe<sub>3</sub>O<sub>4</sub>-1 with 0.65 mg/L of F<sup>−</sup> or 0.15 mg/L of Fe<sup>2+</sup> (or Fe<sup>3+</sup>) under otherwise identical conditions (Figure 5), which supported the notion that the decolorization of OG with H<sub>2</sub>O<sub>2</sub> was catalyzed by heterogeneous F-Fe<sub>3</sub>O<sub>4</sub>-1 solid catalyst, not by soluble species.

The addition of tert-butanol (10 mM) as a scavenger of hydroxyl radicals significantly inhibited the degradation of OG with H<sub>2</sub>O<sub>2</sub> at pH 6.5 over F-Fe<sub>3</sub>O<sub>4</sub>-1. As shown in Figure 6 and Entry 6 in Table 1, the 2 h DR and  $k_{s1}$ , respectively, decreased from 96.8% and 0.0284 min<sup>−1</sup> to 35.2% and 0.0026 min<sup>−1</sup>, implying that hydroxyl radicals are the main reactive oxygen species contributing to the OG degradation. Since the decolorization of OG was not completely suppressed by tert-butanol (10 mM), other reactive oxygen species such as superoxide radical anions may also make a minor contribution to the decolorization of OG.

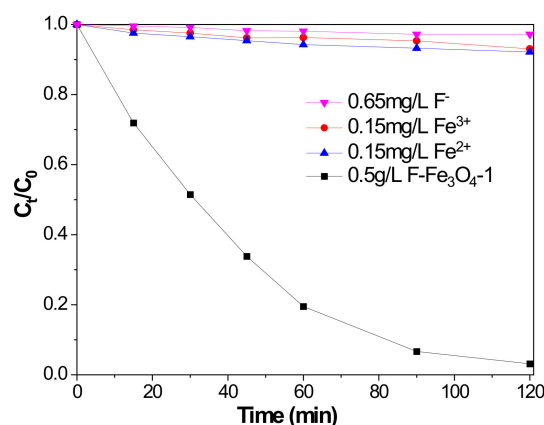


**Figure 5.** Catalytic degradation of OG (0.1 mM, pH 6.5) with H<sub>2</sub>O<sub>2</sub> (40 mM) after replacing 0.5 g/L of F-Fe<sub>3</sub>O<sub>4</sub>-1 with 0.65 mg/L of F<sup>-</sup> or 0.15 mg/L of Fe<sup>2+</sup> (or Fe<sup>3+</sup>).

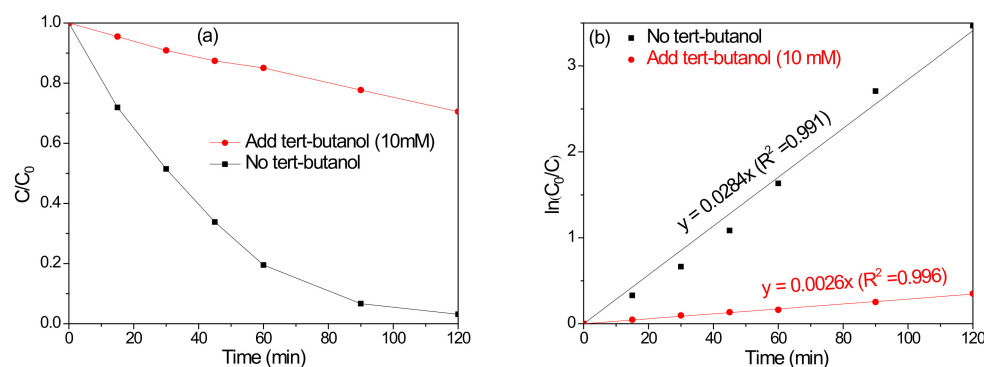


**Figure 6.** Effect of tert-butanol on catalytic degradation of OG with H<sub>2</sub>O<sub>2</sub> over F-Fe<sub>3</sub>O<sub>4</sub>-1. (a)  $C/C_s$ -time plots and (b)  $\ln(C_0/C)$ -time plots. Reaction conditions: OG (0.1 mM, pH 6.5), H<sub>2</sub>O<sub>2</sub> (40 mM), and F-Fe<sub>3</sub>O<sub>4</sub>-1 (0.5 g/L) at 40 °C.

The EPR spectra with the DMPO spin-trapping technique were used to identify the generation of  $\cdot\text{OH}$  radicals. As shown in Figure 7, a typical 1:2:2:1 quadruplet pattern corresponding to the DMPO- $\cdot\text{OH}$  adduct was observed for both F-Fe<sub>3</sub>O<sub>4</sub>-1 and Fe<sub>3</sub>O<sub>4</sub>-blank, supporting the formation of  $\cdot\text{OH}$  radicals in the H<sub>2</sub>O<sub>2</sub>/F-Fe<sub>3</sub>O<sub>4</sub>-1 (or Fe<sub>3</sub>O<sub>4</sub>-blank) reaction system. However, the signal intensities for F-Fe<sub>3</sub>O<sub>4</sub>-1 were obviously stronger than those for Fe<sub>3</sub>O<sub>4</sub>-blank, indicating the higher activity of the former to activate H<sub>2</sub>O<sub>2</sub> due to the larger number of Fe<sup>2+</sup> ions generated after fluorination of F-Fe<sub>3</sub>O<sub>4</sub>-1 [25].

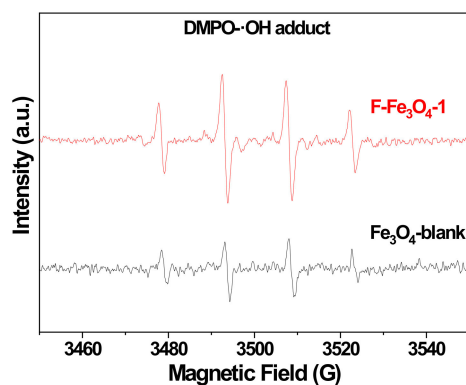


**Figure 7.** DMPO-trapped EPR spectra. Conditions: F-Fe<sub>3</sub>O<sub>4</sub>-1 or Fe<sub>3</sub>O<sub>4</sub>-blank (0.5 g/L), H<sub>2</sub>O<sub>2</sub> (40 mM), and DMPO (ca. 20 mM).



The improved catalytic activity of F-Fe<sub>3</sub>O<sub>4</sub>-1 for the degradation of anionic dyes (e.g., OG and CR) at pH ~7 was related to their enhanced adsorption. According to the measurement of zeta potentials at different pH values (Figure 8), the IEPs of F-Fe<sub>3</sub>O<sub>4</sub>-1 and Fe<sub>3</sub>O<sub>4</sub>-blank were determined to be 8.7 and 4.9, respectively. The higher IEP (8.7) of F-Fe<sub>3</sub>O<sub>4</sub>-1 was attributed to the partial substitution of F<sup>−</sup> for lattice O<sup>2−</sup> in Fe<sub>3</sub>O<sub>4</sub>. As a result, the surface of F-Fe<sub>3</sub>O<sub>4</sub>-1 was positively charged, while Fe<sub>3</sub>O<sub>4</sub>-blank was negatively charged at pH ~7. Therefore, the adsorption of anionic dye molecules on F-Fe<sub>3</sub>O<sub>4</sub>-1 was facilitated via electrostatic attraction but unfavorable on Fe<sub>3</sub>O<sub>4</sub>-blank at pH ~7 due to electrostatic repulsion (e.g., the 15-min adsorption of OG was 5.9% on Fe<sub>3</sub>O<sub>4</sub>-blank vs. 12.3% on F-Fe<sub>3</sub>O<sub>4</sub>-1). It is generally accepted that surface-generated hydroxyl radicals are highly reactive and short-lived [34] and are mostly consumed on the surface before diffusing to the solution [35]. Therefore, the adsorbed anionic molecules (OG or CR), not those in the solution, were more likely to be oxidized by surface-generated hydroxyl radicals. This strengthens the critical role of the adsorption of the solid surface in determining the oxidation rate of pollutants in iron oxide/H<sub>2</sub>O<sub>2</sub> systems [36].

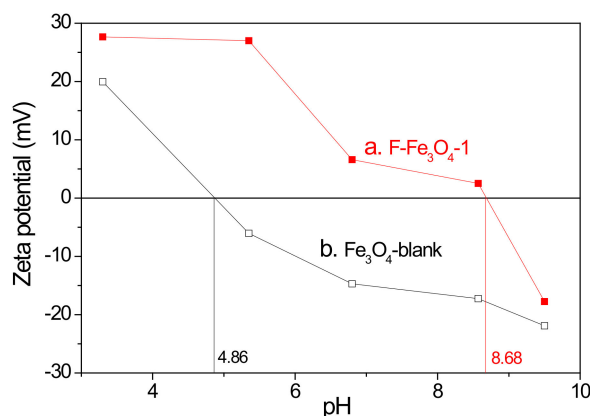


Figure 8. Zeta potentials at different pH values.

### 3. Materials and Methods

#### 3.1. Chemicals and Regents

All chemicals, including FeCl<sub>3</sub>·6H<sub>2</sub>O, NaOAc, NaF, ethylene glycol, orange G (OG), congo Red (CR), methylene blue (MB), rhodamine B (RhB), and 5,5-dimethyl-1-pyrroline N-oxide (DMPO), were of analytic grade or above and used as received. All aqueous solutions were prepared with deionized (DI) water (<20 μS/cm) produced from Heal Force NW 15VF.

#### 3.2. Synthesis of Fluoride-Modified Fe<sub>3</sub>O<sub>4</sub> Microspheres

The fluoride-modified Fe<sub>3</sub>O<sub>4</sub> microspheres were made via glycothermal synthesis according to the reported method [25] and named as F-Fe<sub>3</sub>O<sub>4</sub>-r, where r indicates the nominal F/Fe molar ratio (r: 0–3). The product made at r = 0 was unmodified (denoted Fe<sub>3</sub>O<sub>4</sub>-blank). In brief, NaOAc (22 mmol) and NaF (0–21 mmol) were sequentially added at an interval of 10 min to 4.5 mL of FeCl<sub>3</sub>·6H<sub>2</sub>O (1.5 M) solution in ethylene glycol and then heated in a 60-mL Teflon-lined stainless steel autoclave at 198 °C for 14 h to obtain F-Fe<sub>3</sub>O<sub>4</sub>-r black particles.

#### 3.3. CWPO of Organic Dyes

A general procedure of CWPO was as follows: A mixture of 0.025 g of F-Fe<sub>3</sub>O<sub>4</sub>-r microspheres and 50 mL of OG (C<sub>s</sub> = 0.1 mM) stock solution was first stirred at 750 rpm and 40 ± 2 °C for 15 min to reach the adsorption equilibrium. The concentration of OG was then measured and taken as the concentration at time zero (C<sub>0</sub>). The degradation of OG was initiated by rapidly adding 0.230 g of H<sub>2</sub>O<sub>2</sub> (30%) into the mixture. At selected

intervals, about 3 mL of the samples was taken by a syringe and passed through a filter membrane, and the residual concentration of OG in solution,  $C_t$ , was analyzed. Multiple measurements of the catalytic activity were performed with the relative standard deviation usually below 5%. In recyclability tests, the used F-Fe<sub>3</sub>O<sub>4</sub>-1 was magnetically recovered and directly reused for the next run according to the same procedure. This procedure was also applied to degrade CR, MB, and RhB. The concentrations,  $C_t$ , of OG, CR, MB, and RhB in aqueous solutions were analyzed by measuring the absorbance at 478, 495, 664, and 554 nm, respectively, using a UV-vis spectrophotometer (UV-1800PC, Shanghai Mapada Instrument, Shanghai, China). Before measurement, the pH value of the CR solution in the quartz cuvette was adjusted by adding one drop of 2 wt% KOH.

### 3.4. Physicochemical Characterization

Powder X-ray diffraction (XRD) patterns were collected on Bruker D8 Advance Diffractometer with Cu K $\alpha$  radiation at 30 kV and 20 mA. Scanning electron microscope (SEM) images were taken on JEOL JSM-5510LV SEM (Tokyo, Japan) at 20 kV. N<sub>2</sub> adsorption-desorption isotherms were measured on Micromeritics ASAP 2020 (Georgia, United States) at 77 K. The samples were degassed under vacuum at 100 °C for 2 h before measurements. The BET specific surface area  $S_{\text{BET}}$  was calculated from the adsorbed quantities in the relative pressure ( $P/P_0$ ) range of 0.05–0.30. M-H curves were measured on a JDAW-2000D (Jilin, China) vibrating sample magnetometer (VSM) at room temperature. Zeta potentials were determined at different pH values on Malvern Zetasizer Zen3690 (Malvern, United Kingdom). Electron-spin resonance (EPR) spectra were collected on Bruker EMXplus (Berlin, Germany) at room temperature. The concentrations of fluoride and iron ions in the solution were analyzed using ionic chromatography (ICS-1500) and atomic absorption spectroscopy (Agilent 240 AA, California, United States), respectively.

## 4. Conclusions

Fluorination increased the isoelectric point from 4.9 for undoped Fe<sub>3</sub>O<sub>4</sub>-blank microspheres to 8.7 for F-Fe<sub>3</sub>O<sub>4</sub>-1 with  $7.1 \pm 1.4$  wt% of fluoride. In comparison with Fe<sub>3</sub>O<sub>4</sub>-blank, F-Fe<sub>3</sub>O<sub>4</sub>-1 could efficiently catalyze the decolorization of anionic dye solutions at pH ~7. This was mainly attributed to the enhanced adsorption of anionic dyes on the surface of F-Fe<sub>3</sub>O<sub>4</sub>-1 via electrostatic attraction, followed by oxidative degradation via a free-radical reaction pathway. This work strengthens the critical role of the adsorption of the solid surface in determining the oxidation rate of pollutants in iron oxide/H<sub>2</sub>O<sub>2</sub> systems.

**Supplementary Materials:** The following supporting information can be downloaded at: <https://www.mdpi.com/article/10.3390/catal12121564/s1>, Figure S1: The Arrhenius plot of the degradation of OG (0.1 mM, pH 6.5) with H<sub>2</sub>O<sub>2</sub> on F-Fe<sub>3</sub>O<sub>4</sub>-1 microspheres; Table S1: Effect of initial H<sub>2</sub>O<sub>2</sub> concentration on OG decolorization with H<sub>2</sub>O<sub>2</sub> over F-Fe<sub>3</sub>O<sub>4</sub>-1 microspheres; Table S2: Effect of initial pH on OG decolorization with H<sub>2</sub>O<sub>2</sub> over F-Fe<sub>3</sub>O<sub>4</sub>-1 microspheres; Table S3: Effect of reaction temperature on OG decolorization with H<sub>2</sub>O<sub>2</sub> over F-Fe<sub>3</sub>O<sub>4</sub>-1 microspheres; and Table S4: EDX-determined elemental composition of F-Fe<sub>3</sub>O<sub>4</sub>-1 microspheres.

**Author Contributions:** Conceptualization, F.C.; methodology, investigation, data curation, and formal analysis, H.L., W.C. and F.C.; resources, F.C. and R.C.; and writing—original draft preparation, review, and editing, F.C. All authors have read and agreed to the published version of the manuscript.

**Funding:** This work was supported by National Natural Science Foundation of China (No. 21571146).

**Data Availability Statement:** Data are available within the article.

**Conflicts of Interest:** The authors declare no conflict of interest.

## References

1. Ribeiro, R.S.; Silva, A.M.T.; Figueiredo, J.L.; Faria, J.L.; Gomes, H.T. Catalytic wet peroxide oxidation: A route towards the application of hybrid magnetic carbon nanocomposites for the degradation of organic pollutants. A review. *Appl. Catal. B Environ.* **2016**, *187*, 428–460. [CrossRef]

2. Munoz, M.; de Pedro, Z.M.; Casas, J.A.; Rodriguez, J.J. Preparation of magnetite-based catalysts and their application in heterogeneous Fenton oxidation—A review. *Appl. Catal. B Environ.* **2015**, *176*–177, 249–265. [\[CrossRef\]](#)
3. Huang, R.; Fang, Z.; Yan, X.; Cheng, W. Heterogeneous sono-Fenton catalytic degradation of bisphenol A by Fe<sub>3</sub>O<sub>4</sub> magnetic nanoparticles under neutral condition. *Chem. Eng. J.* **2012**, *197*, 242–249. [\[CrossRef\]](#)
4. Pham, A.L.-T.; Lee, C.; Doyle, F.M.; Sedlak, D.L. A silica-supported iron oxide catalyst capable of activating hydrogen peroxide at neutral pH values. *Environ. Sci. Technol.* **2009**, *43*, 8930–8935. [\[CrossRef\]](#) [\[PubMed\]](#)
5. Zhu, Y.; Zhu, R.; Xi, Y.; Zhu, J.; Zhu, G.; He, H. Strategies for enhancing the heterogeneous Fenton catalytic reactivity: A review. *Appl. Catal. B Environ.* **2019**, *255*, 117739. [\[CrossRef\]](#)
6. Pouran, S.R.; Raman, A.A.A.; Daud, W.M.A.W. Review on the application of modified iron oxides as heterogeneous catalysts in Fenton reactions. *J. Clean. Prod.* **2014**, *64*, 24–35. [\[CrossRef\]](#)
7. Bokare, A.D.; Choi, W. Review of iron-free Fenton-like systems for activating H<sub>2</sub>O<sub>2</sub> in advanced oxidation processes. *J. Hazard. Mater.* **2014**, *275*, 121–135. [\[CrossRef\]](#)
8. Yin, Y.; Shi, L.; Li, W.; Li, X.; Wu, H.; Ao, Z.; Tian, W.; Liu, S.; Wang, S.; Sun, H. Boosting Fenton-like reactions via single atom Fe catalysis. *Environ. Sci. Technol.* **2019**, *53*, 11391–11400. [\[CrossRef\]](#)
9. Gao, L.; Zhuang, J.; Nie, L.; Zhang, J.; Zhang, Y.; Gu, N.; Wang, T.; Feng, J.; Yang, D.; Perrett, S.; et al. Intrinsic peroxidase-like activity of ferromagnetic nanoparticles. *Nat. Nanotechnol.* **2007**, *2*, 577–583. [\[CrossRef\]](#)
10. Chen, F.; Xie, S.; Huang, X.; Qiu, X. Ionothermal synthesis of Fe<sub>3</sub>O<sub>4</sub> magnetic nanoparticles as efficient heterogeneous Fenton-like catalysts for degradation of organic pollutants with H<sub>2</sub>O<sub>2</sub>. *J. Hazard. Mater.* **2017**, *322*, 152–162. [\[CrossRef\]](#)
11. Huang, X.; Xu, C.; Ma, J.; Chen, F. Ionothermal synthesis of Cu-doped Fe<sub>3</sub>O<sub>4</sub> magnetic nanoparticles with enhanced peroxidase-like activity for organic wastewater treatment. *Adv. Powder Technol.* **2018**, *29*, 796–803. [\[CrossRef\]](#)
12. Xu, C.; Zhang, J.; Huang, X.; Chen, F. One-step nonaqueous synthesis of modified magnetic Fe<sub>3</sub>O<sub>4</sub> microspheres by using epichlorohydrin as functional solvent. *Chem. Lett.* **2019**, *48*, 22–25. [\[CrossRef\]](#)
13. Huang, X.; Du, W.; Chen, R.; Chen, F. Adsorption-enhanced catalytic wet peroxide oxidation of aromatic compounds on ionothermally synthesised copper-doped magnetite magnetic nanoparticles. *Environ. Chem.* **2020**, *17*, 426–435. [\[CrossRef\]](#)
14. Liang, X.; Zhong, Y.; He, H.; Yuan, P.; Zhu, J.; Zhu, S.; Jiang, Z. The application of chromium substituted magnetite as heterogeneous Fenton catalyst for the degradation of aqueous cationic and anionic dyes. *Chem. Eng. J.* **2012**, *191*, 177–184. [\[CrossRef\]](#)
15. Wang, J.; Zheng, S.; Shao, Y.; Liu, J.; Xu, Z.; Zhu, D. Amino-functionalized Fe<sub>3</sub>O<sub>4</sub>@SiO<sub>2</sub> core-shell magnetic nanomaterial as a novel adsorbent for aqueous heavy metals removal. *J. Colloid Interf. Sci.* **2010**, *349*, 293–299. [\[CrossRef\]](#)
16. Cai, H.; Li, X.; Ma, D.; Feng, Q.; Wang, D.; Liu, Z.; Wei, X.; Chen, K.; Lin, H.; Qin, S.; et al. Stable Fe<sub>3</sub>O<sub>4</sub> submicrospheres with SiO<sub>2</sub> coating for heterogeneous Fenton-like reaction at alkaline condition. *Sci. Total Environ.* **2021**, *764*, 14420. [\[CrossRef\]](#)
17. Zhang, J.; Wang, Z.; Chen, R.; Chen, F. New soft chemistry route to titanomagnetite magnetic nanoparticles with enhanced peroxidase-like activity. *Powder Technol.* **2020**, *373*, 39–45. [\[CrossRef\]](#)
18. Du, W.; Huang, R.; Huang, X.; Chen, R.; Chen, F. Copper-promoted heterogeneous Fenton-like oxidation of Rhodamine B over Fe<sub>3</sub>O<sub>4</sub> magnetic nanocatalysts at mild conditions. *Environ. Sci. Pollut. Res.* **2021**, *28*, 19959–19968. [\[CrossRef\]](#)
19. Yu, J.C.; Yu, J.; Ho, W.K.; Jiang, Z.; Zhang, L. Effects of F-doping on the photocatalytic activity and microstructures of nanocrystalline TiO<sub>2</sub> powders. *Chem. Mater.* **2002**, *14*, 3808–3816. [\[CrossRef\]](#)
20. Kumar, V.; Govind, A.; Nagarajan, R. Optical and photocatalytic properties of heavily F<sup>−</sup>-doped SnO<sub>2</sub> nanocrystals by a novel single-source precursor approach. *Inorg. Chem.* **2011**, *50*, 5637–5645. [\[CrossRef\]](#)
21. Gasparotto, A.; Barreca, D.; Bekermann, D.; Devi, A.; Fischer, R.A.; Fornasiero, P.; Gombac, V.; Lebedev, O.I.; Maccato, C.; Montini, T.; et al. F-doped Co<sub>3</sub>O<sub>4</sub> photocatalysts for sustainable H<sub>2</sub> generation from water/ethanol. *J. Am. Chem. Soc.* **2011**, *133*, 19362–19365. [\[CrossRef\]](#) [\[PubMed\]](#)
22. Zhu, L.-P.; Wang, L.-L.; Bing, N.-C.; Huang, C.; Wang, L.-J.; Liao, G.-H. Porous fluorine-doped γ-Fe<sub>2</sub>O<sub>3</sub> hollow spheres: Synthesis, growth mechanism, and their application in photocatalysis. *ACS Appl. Mater. Interfaces* **2013**, *5*, 12478–12487. [\[CrossRef\]](#) [\[PubMed\]](#)
23. Yu, L.; Xiong, L.; Yu, Y. Cu<sub>2</sub>O homojunction solar cells: F-doped n-type thin film and highly improved efficiency. *J. Phys. Chem. C* **2015**, *119*, 22803–22811. [\[CrossRef\]](#)
24. Fu, H.; Zhang, S.; Xu, T.; Zhu, Y.; Chen, J. Photocatalytic degradation of RhB by fluorinated Bi<sub>2</sub>WO<sub>6</sub> and distributions of the intermediate products. *Environ. Sci. Technol.* **2008**, *42*, 2085–2091. [\[CrossRef\]](#)
25. Chen, W.; Zhang, J.; Chen, F. Glycothermal synthesis of fluorinated Fe<sub>3</sub>O<sub>4</sub> microspheres with distinct peroxidase-like activity. *Adv. Powder Technol.* **2019**, *30*, 999–1005. [\[CrossRef\]](#)
26. Luo, W.; Zhu, L.; Wang, N.; Tang, H.; Cao, M.; She, Y. Efficient removal of organic pollutants with magnetic nanoscaled BiFeO<sub>3</sub> as a reusable heterogeneous Fenton-like catalyst. *Environ. Sci. Technol.* **2010**, *44*, 1786–1791. [\[CrossRef\]](#)
27. Xue, X.; Hanna, K.; Deng, N. Fenton-like oxidation of Rhodamine B in the presence of two types of iron (II, III) oxide. *J. Hazard. Mater.* **2009**, *166*, 407–414. [\[CrossRef\]](#)
28. Dean, J.A. *Lange's Handbook of Chemistry*, 15th ed.; McGraw-Hill: New York, NY, USA, 1998.
29. Wang, N.; Zhu, L.; Wang, M.; Wang, D.; Tang, H. Sono-enhanced degradation of dye pollutants with the use of H<sub>2</sub>O<sub>2</sub> activated by Fe<sub>3</sub>O<sub>4</sub> magnetic nanoparticles as peroxidase mimetic. *Ultrason. Sonochem.* **2010**, *17*, 78–83. [\[CrossRef\]](#)
30. Lin, C.-C.; Ho, J.-M.; Hsieh, H.-L. Feasibility of using a rotating packed bed in preparing Fe<sub>3</sub>O<sub>4</sub> nanoparticles. *Chem. Eng. J.* **2012**, *203*, 88–94. [\[CrossRef\]](#)

31. Anandkumar, J.; Mandal, B. Adsorption of chromium(VI) and Rhodamine B by surface modified tannery waste: Kinetic, mechanistic and thermodynamic studies. *J. Hazard. Mater.* **2011**, *186*, 1088–1096. [[CrossRef](#)]
32. Chen, F.; Zhao, J.; Hidaka, H. Highly selective deethylation of rhodamine B: Adsorption and photooxidation pathways of the dye on the TiO<sub>2</sub>/SiO<sub>2</sub> composite photocatalyst. *Int. J. Photoenergy* **2003**, *5*, 209–217. [[CrossRef](#)]
33. Guo, Y.; Zhao, J.; Zhang, H.; Yang, S.; Qi, J.; Wang, Z.; Xu, H. Use of rice husk-based porous carbon for adsorption of Rhodamine B from aqueous solutions. *Dye. Pigment.* **2005**, *66*, 123–128. [[CrossRef](#)]
34. Guo, S.; Wang, H.; Yang, W.; Fida, H.; You, L.; Zhou, K. Scalable synthesis of Ca-doped  $\alpha$ -Fe<sub>2</sub>O<sub>3</sub> with abundant oxygen vacancies for enhanced degradation of organic pollutants through peroxymonosulfate activation. *Appl. Catal. B Environ.* **2020**, *262*, 118250. [[CrossRef](#)]
35. Lin, S.-S.; Gurol, M.D. Catalytic decomposition of hydrogen peroxide on iron oxide: Kinetics, mechanism, and implications. *Environ. Sci. Technol.* **1998**, *32*, 1417–1423. [[CrossRef](#)]
36. Hanna, K.; Kone, T.; Medjahdi, G. Synthesis of the mixed oxides of iron and quartz and their catalytic activities for the Fenton-like oxidation. *Catal. Commun.* **2008**, *9*, 955–959. [[CrossRef](#)]